An Overview of Recent Results from CLAS

Kenneth H. Hicks[1] on behalf of the CLAS Collaboration
Department of Physics and Astronomy, Ohio University
Athens, Ohio 45701, USA

The unique capabilities of the CLAS detector to measure exclusive meson electroproduction off protons, with almost complete coverage of the final hadron phase space, has extended our knowledge of excited baryon structure. Consistent results from $N\pi$ and $N\pi\pi$ final states provide convincing evidence for reliable extraction of N* electrocouplings. Theoretical analyses of these results, using self-consistent dynamical calculations using an internal quark core and an external meson-baryon cloud suggest that meson-baryon dressing amplitudes need to be included. The meson-baryon dressing was already shown to be necessary to get agreement between calculations and data on the Δ resonance transition magnetic moment at low Q^2. Similarly, a new measurement of the transition magnetic moment for strange baryons also disagrees with quark models, suggesting the need for meson-baryon dressings. In the near future, the CLAS detector will be replaced with CLAS12, providing new high-precision data.

1 Introduction

With the goal of understanding the resonance structure of the nucleon, the CLAS Detector [1] has measured a variety of electron and photon scattering reactions off a proton target. The resulting data provide a wealth of information about the electrocouplings of nucleon resonances at photon four-momentum transfers ranging up to $Q^2 < 5\,\mathrm{GeV}^2$. In addition, the electromagnetic decay of baryon resonances having strangeness, such as the Σ* resonance at mass 1385 GeV/c^2, have been measured for the first time due to the high luminosity and large acceptance of the CLAS experiments. Both of these phenomena point toward the active role of a meson-baryon cloud as part of the wave-function describing baryon resonances. Theoretical progress made by the Excited Baryon Analysis Center (EBAC) at Jefferson Lab provides calculations that allow interpretation of the experimental data using a dynamical coupled channels model [2–4] that includes a bare N* core and its fluctuation into a meson-baryon cloud. Superposition of the amplitues from the meson-baryon cloud and the quark core predicts measureable effects in the N* electrocouplings. With the advent of high precision data from CLAS and other facilities around the world, these theoretical ideas can be tested and have led to a better understanding of baryon resonances.

---

[1]hicks@ohio.edu

One of the major breakthroughs of recent years in the understanding of QCD is the non-perturbative calculations using the Dyson-Schwinger equation (DSE) [5]. Shown in Fig. 1 is the quark mass as a function of the momentum variable q of the dressed quark propagator. When the quark is hit hard, giving the propagator a momentum greater than about 1 GeV, the effective quark mass becomes very small, while for soft interactions, the quark becomes "dressed" with a gluon cloud, attaining an effective mass (even in the chiral limit) of about 1/3 of the nucleon mass. Fig. 1 also shows data from lattice gauge calculations for light quark masses, which agrees with the curves from the DSE approach with the same input quark mass. The lesson to take away is that 97% of the dressed quark mass comes from the gluon dressing of the bare (core) quark in the regime of large quark-gluon coupling. Hence quarks should not be assigned a fixed mass (as is done in the non-relativistic constituent quark model), especially when probing high momentum transfer reactions. Furthermore, because gluons couple to quark-antiquark loops, the gluon cloud also has virtual meson components.

Non-perturbative interactions of dressed quarks and gluons create a quark core of both ground and excited states of the proton. On top of that, we have the contribution from an external meson-baryon cloud, required by the general unitarity condition for meson-baryon interaction amplitudes [4].

An example of the importance of meson-baryon effects is shown in Fig. 2, where data on the magnetic dipole transition form factor, $G_M(Q^2)$, for $\gamma^* N \to \Delta$ transitions is shown as a function of the virtual photon 4-momentum, Q^2. At low Q^2, the solid (dashed) curve calculated with (without) the baryon dressing show a significant contribution of the meson-baryon cloud to this observable [6]. In the non-relativistic quark model, the value of $G_M(0)$ is directly proportional to the proton magnetic moment, and the value of G_M extrapolate to $Q^2 = 0$ can only be explained in that model if the experimental magnetic moment is lowered by about 30%. Without the meson-baryon cloud effects, this simple theoretical model is in direct contradiction with experimental facts. Hence there is a need for dynamical meon-baryon amplitudes to explain the electrocoupling to the best known nucleon resonance, the Δ. It should not be a surprise if dynamical meson-baryon effects are also necessary to explain electrocouplings to other baryon resonances.

In the following sections, experimental results from CLAS using virtual photons, including both single and double pion-production reactions, are compared with theoretical models and the magnitude of the meson-baryon dressing amplitudes. Next, the electromagnetic decay of baryons with strangeness are described, showing strong evidence for effects from the meson-baryon cloud. A short recap of the search for exotic mesons and glueball-mixing at CLAS is provided, followed by a description of the planned upgrade to 12 GeV beam energies and the new CLAS12 detector at Jefferson Lab.
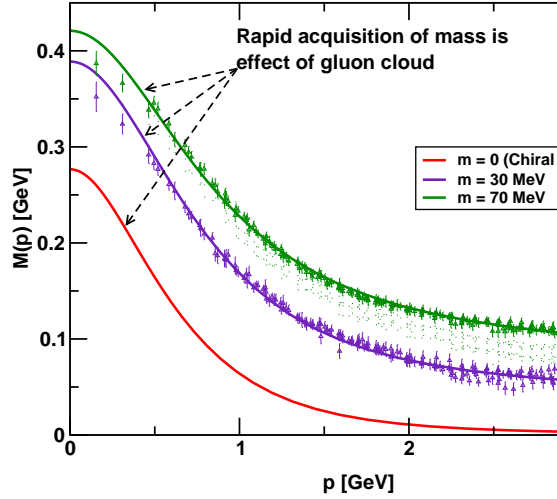
Figure 1: Calculations of the quark effective mass as a function of the quark momentum using the Dyson-Schwinger equation, from Ref. [5].

2 Experimental Description and Results

The measurements reported here were done using the high intensity electron beam with energies up to 6 GeV with 100% duty cycle from the Continuous Electron Beam Accelerator Facility (CEBAF), located at the Thomas Jefferson National Accelerator Facility in the USA. CEBAF has the shape of a racetrack, with two superconducting RF-linacs along the straight sections and groups of normal conducting magnets along the recirculation arcs. The electron beam can be circulate around the linacs up to five times, gaining approximately 1.2 GeV on each pass (a distance of about 1.4 km). The beam can be sent simultaneously to three experimental halls: A, B and C.

The CEBAF Large Acceptance Spectrometer (CLAS), housed in Hall B, is shown in Fig. 3. Both electron and tagged photon beams can be directed onto the target, shown in the center of the cutaway region of the figure. Surrounding the target is a toroidal magnetic field generated by six superconducting coils spaced uniformly in angle about the beamline axis. Within each of the six sectors, there are multiple layers of drift chambers, spaced radially outward from the target, to track the outgoing particles. For photon beam experiments, a segmented scintillator called the start counter surrounds the target, providing timing
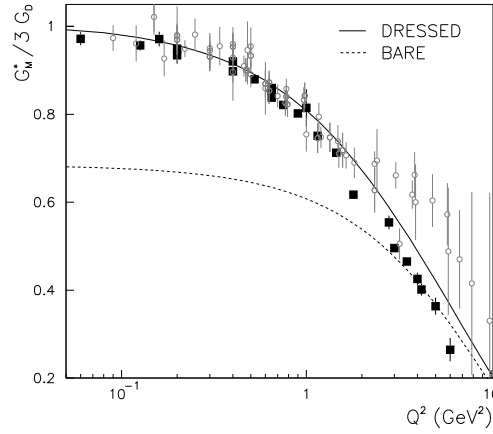
Figure 2: The transition magnetic moment G_M, in units of the proton dipole form factor as a function of Q^2 for the $\gamma^* N \to \Delta$ electromagnetic transition, from Ref. [6].

information for charged particles and forms part of the trigger in coincidence with the tagged electron. Outside of the three regions of drift chambers, a gas Cerenkov counter identifies electrons and helps to discriminate pions from electrons. The whole system is surrounded by a layer of plastic scintillator bars to record the time-of-flight (TOF) of particles from the target. At the outermost layer, shown by the triangular sections in Fig. 3, is the electromagnetic calorimeter, made from alternating layers of plastic scintillator and thin lead sheets, used for detection of electrons, photons and (for some experiments) neutrons.

For all data presented below, the target was a liquid hydrogen cell. A typical luminosity for electron running was about $10^{34}/\text{cm}^2/\text{s}$ and for photon experiments, the rate on a typical 40 cm target was about 10^7 photons/sec, integrated from 10% to 95% of the electron beam energy, in a classic bremsstrahlung distribution. Both beams and target can be polarized, which provides additional information for partial wave analysis of scattering reactions. Complete sets of polarization measurements are the next step in a series of results coming from CLAS data, with the goal of isolating spin-dependent amplitudes in production of baryon resonances.

Fig. 4 shows the electrocoupling of the $P_{11}(1440)$ resonance. Using a total of about 12000
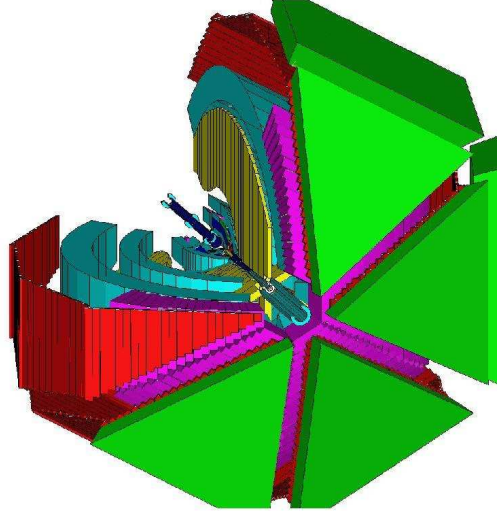
Figure 3: Schematic diagram of CLAS detector, with one region cut away to show the inner structure of detectors.

data points on differential cross sections, from experiments using both unpolarized beams or longitudinal polarization of beam and/or target, CLAS has the most complete coverage of the kinematics corresponding to the Roper resonance, centered at 1440 MeV with a width of several hundred MeV. More information on the data set, including electrocouplings to the $S_{11}(1535)$ resonance, can be found in Ref. [7]. The data shown in Fig. 4 are for the $A_{1/2}$ amplitude, scaled up by a factor of 1000, where the open symbols for $Q^2 > 0$ are from single pion electroproduction data (both $\pi^+ n$ and $\pi^0 p$) and the closed symbols [8] are from two-pion electroproduction ($\pi^+\pi^- p$) data [9]. Points at $Q^2 = 0$ are from high-precision single-pion photoproduction data [10].

Consistent results on electrocouplings of the $P_{11}(1440)$ and $D_{13}(1530)$ resonances obtained in independent analyses of two major meson electroproduction channels ($N\pi$ and $N\pi\pi$) with different non-resonant contributions clearly show the reliable extraction of these fundamental quantities. Furthermore, the reaction models [7] for extraction of N^* electrocouplings from independent analyses of $N\pi$ and $p\pi^+\pi^-$ channels allows a determination of electrocouplings of all resonances that decay preferentially to these final state. Preliminary results on electrocouplings of $S_{31}(1620)$, $S_{11}(1650)$, $F_{15}(1685)$, $D_{33}(1700)$ and $P_{13}(1720)$ states were obtained [7] from the CLAS data on $p\pi^+\pi^-$ electroproduction data within the theoretical
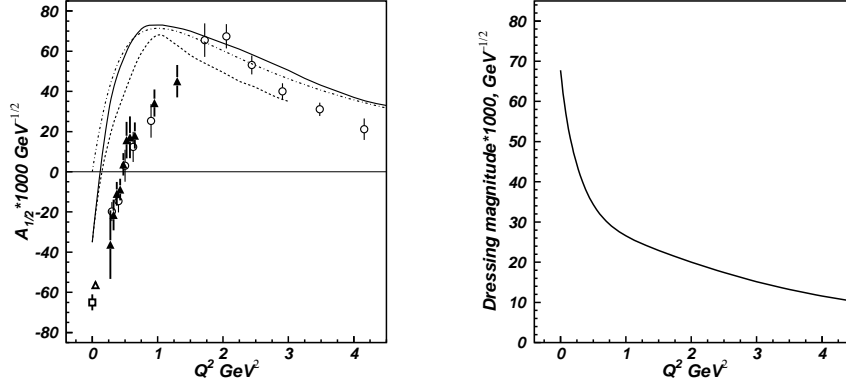
Figure 4: Left: Electrocoupling of the $P_{11}(1440)$ resonance; right: calculated magnitude of the meson-baryon dressing amplitudes for the same resonance. See text for discussion of symbols and curves.

framework discussed in Ref. [11].

The curves in the left panel of Fig. 4 are from light-front quark models [12, 13] (solid and dashed) and from a diquark model [14] (dot-dashed). These curves all follow the general trend of the data, but fail to predict the data at low Q^2. One explanation may be that the curves in the left panel do not include meson-baryon dressing, which is calculated within the dynamical coupled-channels model [3], with its magnitude shown in the right panel of Fig. 4. As shown in the previous figure, the meson-baryon dressing has a substantial effect on theoretical calculations of Δ-resonance transition magnetic moments, and a similarly large effect of the dressing is calculated for the Roper resonance shown in Fig. 4.

Further evidence for the importance of the meson-baryon cloud comes from electromagnetic decay of excited strange baryons. Recent analysis of CLAS data for the reaction $\gamma p \to K\Sigma^*$ provides high statistics for the Σ^* resonance, a decuplet baryon with strangeness -1. The Σ^* can decay via the strong force to $\Sigma\pi^0$ or via electromagnetic (EM) decay to $\Sigma\gamma$. The latter is expected to have a branching ratio of about 1%, and hence is difficult to measure. Just like the Δ transition magnetic moment discussed above, the EM decay of the Σ^* holds information on the effect of the meson-baryon cloud. Previously reported CLAS data for the EM decay $\Sigma^{*0} \to \Lambda\gamma$ has already shown that this is an important effect [15].

The missing mass for $\gamma p \to K^0\Sigma^+ X$ is shown [16] in Fig. 5 where the upper histogram is for all data (after cuts to isolate the given final state) with a prominant peak at the mass of the π^0
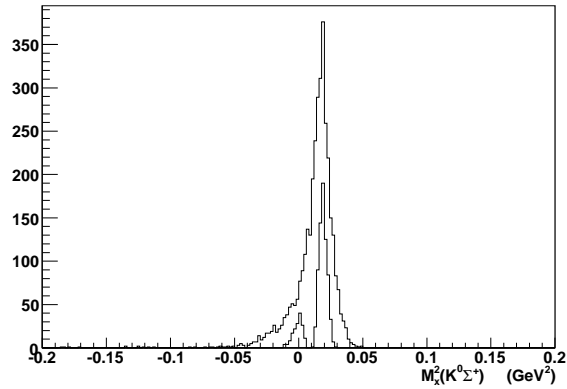
Figure 5: Missing mass of the reaction $\gamma p \rightarrow K^0 \Sigma^+ X$ from CLAS data [16].

and a "shoulder" at zero mass corresponding to γ decay. By use of a sophisticated kinematic fit, which can be shown to be robust in its ability to extract the ratio of EM to strong decay of the Σ^{*+}, the lower histograms in Fig. 5 are the result, showing a clean separation of these two decays. This is the world's first extraction of the EM decay branching ratio for the Σ^{*+}, which provides a test of the meson-baryon cloud for baryons with strangeness. The results are shown in Table 1, where the experimentally extracted transition magnetic moments ($Q^2 = 0$) are compared with the first-order $1/N_c$ expansion of Jenkins and Manohar [17] and the naive quark model [18]. Both theoretical models substantially underpredict the experimentally measured values, similar to the case of the Δ transition magnetic moment [6].

While CLAS has provided world-class data, resulting in the world's best extractions of electrocouplings and transition magnetic moments, this detector will be dismantled in 2012 and replaced with a new detector, CLAS12, for operation with the energy upgrade of CEBAF to 12 GeV. A computer drawing of the CLAS12 detector is shown in Fig. 6. The main features of CLAS12 is its ability to take data at luminosities higher by an order of

7

Transitions	$1/N_c$ Model	Quark Model	Experiment
$\mu_{\Sigma\Sigma*+}$	2.17 ± 0.30	2.33	3.22 ± 0.35
$\mu_{\Lambda\Sigma*0}$	2.28 ± 0.32	2.28	2.75 ± 0.23

Table 1: Transition magnetic monemts of the $\Sigma(1385)$ from the $1/N_c$ and naive quark model compared with the CLAS experimental results.

magnitude than the present CLAS detector. In addition, CLAS12 has improved particle identification, along with tracking at angles as small as $5°$ in the laboratory frame.

There are two major parts to the CLAS12 detector: the Central Detector, which includes a superconducting solenoid (shown in the left part of Fig. 6) and the Forward Detector, which includes a six-sector toroidal magnetic field (shown in the middle of Fig. 6). Inside the solenoid will be a silicon vertex tracker (SVT) and central time-of-flight detectors (CTOF). At forward angles will be a high-threshold and a low-threshold Cerenkov detector (HTCC and LTCC), 3 regions of drift chambers (DC), forward time-of-flight scintillators (FTOF), a pre-shower calorimeter (PCAL) and an electromagnetic calorimeter (EC). Not visible is a low-angle inner calorimeter (IC) for detection of high-energy photons.

The primary physics goals of CLAS12 is to measure: Generalized Parton Distributions (GPDs), Transverse Momentum Distributions (TMDs), hadronization in Deep Inelastic Scattering (DIS), meson spectroscopy and studies of N^* structure at photon virtualities of $Q^2 > 5.0\,\text{GeV}^2$. Each of these topic will be discussed briefly below.

GPDs were introduced about a decade ago, using a theoretical approximation valid for hard-quark scattering that has proven to be extremely efficient at describing experimental data. Leading order Feynmann diagrams for GPDs (also called "handbag" diagrams) describe the correlations between the helicity, longitudinal momentum and transverse position of quarks in the nucleon. Two spin-independent GPDs (H and E) and two spin-dependent GPDs ($\tilde{H}$ and $\tilde{E}$) are accessible through exclusive hard reactions such as Deeply Virtual Compton Scattering (DVCS) measurements using the CLAS12 detector.

TMDs can be accessed via semi-inclusive deep inelastic scattering (SIDIS) where a meson is detected along with a scattered electron. Using polarized beams and polarized targets, TMDs such as the Sivers and Boer-Mulders functions provide information about the momentum distribution of the quarks transverse to the beam direction. Non-zero values for these functions are related to the orbital angular momentum of the quarks, which contribute to the overall nucleon spin. The future CLAS12 data will provide unprecidented precision of the TMDs, resulting in better knowledge of the quark momentum distributions in the nucleon.

Studies of nucleon resonances at the largest photon virtualities ever achieved, from Q^2 of 5 to $12\,\text{GeV}^2$, will allow us for the first time to access almost directly the quark degrees of freedom in N^* structure. It will also allow us to explore the origin of the dynamical
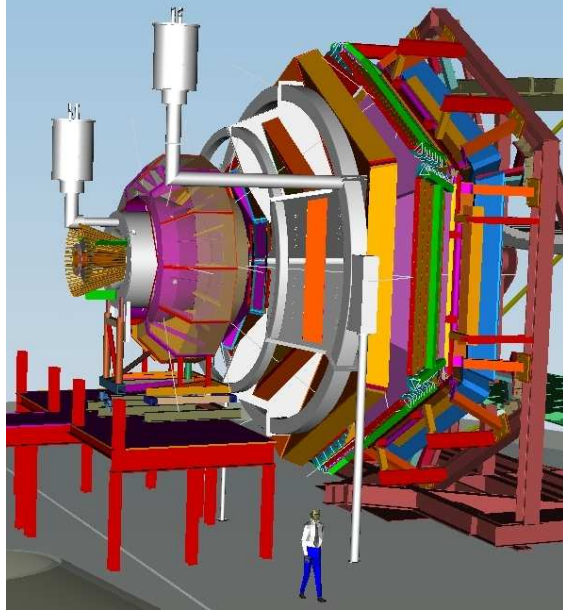
Figure 6: Schematic drawing of the CLAS12 detector, which will soon be installed in Hall B, replacing the CLAS detector.

mass and structure of dressed quarks, along with the non-perturbative strong interactions coming from QCD that are responsible for nucleon structure [19].

3 Summary

Effects of the meson-baryon clould are now evident from the analysis of high-precision data from CLAS. Such effects are expected theoretically from calculations using the Dyson-Schwinger equation, where the effective quark mass changes with Q^2. Experimentally, data from electroproduction of nucleon resonances, such as the Δ and Roper resonances, show clear deviations from calculations with no meson-baryon cloud. For the Δ, agreement is again achieved for dynamical calculations that include the meson-baryon cloud. For the $P_{11}(1440)$, the magnitude of the meson-baryon cloud effects are consistent with the difference between measured electrocouplings and light-front quark models. Decuplet-octet transition magnetic moments of the strange baryons also disagree with quark model calculations, pointint to the need for dynamical coupled-channels calculations that include the meson-baryon cloud.

Future measurements with the CLAS12 detector, which will replace the CLAS detector for the planned 12 GeV energy upgrade at Jefferson Lab, open new possibilities to measure GPDs and TMDs using polarized beams and polarized targets. These data will provide new information on, amoung other things, the orbital angular momentum of quarks inside the nucleon and correlations between momentum and position of these quarks. A rich physics program awaits the measurements that will be done with CLAS12.

Acknowledgments

References

[1] B. Mecking *et al.*, NIM A **503**, 513 (2003).

[2] A. Matsuyama, T. Sato, and T.-S.H. Lee, Phys. Rep. **439** 193 (2007).

[3] B. Julia-Diaz *et al.*, Phys. Rev. C **77**, 045205 (2008).

[4] N. Suzuki *et al.*, Phys. Rev. C **82**, 045206 (2010).

[5] M.S. Bhagwat, I.C. Cloët and C.D. Roberts, in *Exclusive Reactions at High Momentum Transfer*, A. Radyushkin and P. Stoler, eds. (World Scientific, Singapore, 2008), pp. 112-120.

[6] B. Julia-Diaz, T.-S.H. Lee, A. Matsuyama and L.C. Smith Phys. Rev. C **77**, 045205 (2008).

[7] I.G. Aznauryan *et al.*, Phys. Rev. C **80**, 055203 (2009).

[8] I.G. Aznauryan, V.D. Burkert, V.I. Mokeev, arXiv:1108.1125.

[9] G.V. Fedotov *et al.*, Phys. Rev. C **79**, 015204 (2009).

[10] M. Dugger *et al.*, Phys. Rev. C **79**, 065206 (2009).

[11] V.I. Mokeev *et al.*, Phys. Rev. C **80**, 045212 (2009).

[12] I.G. Aznauryan, Phys. Rev. C **76**, 025212 (2007).

[13] S. Capstick and B.D. Keister, Phys. Rev. D **51**, 3598 (1995).

[14] G. Ramalho and K. Tsushima, Phys. Rev. D **81**, 074020 (2010).

[15] D. Keller, *et al.*, Phys. Rev. D **83**, 072004 (2011).

[16] D. Keller, *et al.*, submitted to Phys. Rev. D.

[17] E. Jenkins and A.V. Manohar, Phys. Lett. B **335**,452 (1994).

[18] R. Dhir and R.C. Verma, Eur. Phy. J. A **42**, 243-249 (2010).

[19] I.G. Aznauryan *et al.*, arXiv:0907.1901.